Moreover

$$\partial^\dagger \partial = \partial_1^2 + \partial_2^2 = \triangle \ . \tag{2.69}$$

Thus,

$$\partial^\dagger \partial \hat{\Psi} = \triangle \hat{\Psi} = 2\kappa \ . \tag{2.70}$$

Note that while $\hat{\Psi}$ is a spin-0 scalar field, the application of the ∂ operator generate the deflection angle, i.e. a spin-1 vector field. On the contrary, the $\partial^\dagger$ operator applied to the deflection field lower it to another spin-0 scalar field (the convergence). Therefore, the ∂ and $\partial^\dagger$ operators can be considered as spin raising and lowering operators.

By applying twice the raising operator, we obtain

$$\frac{1}{2}\partial\partial\hat{\Psi} = \frac{1}{2}\partial\alpha = \gamma \ : \tag{2.71}$$

the shear field is indeed a spin-2 tensor field, which is invariant for rotations by multiples of π.

Note also that

$$\partial^{-1}\partial^\dagger\gamma = \frac{1}{2}\partial^{-1}\partial^\dagger\partial\partial\hat{\Psi} = \partial^\dagger\partial\hat{\Psi} = \kappa \tag{2.72}$$

We can use the raising and lowering operators to define

$$F = \frac{1}{2}\partial\partial^\dagger\partial\hat{\Psi} = \partial\kappa \tag{2.73}$$

$$G = \frac{1}{2}\partial\partial\partial\hat{\Psi} = \partial\gamma \tag{2.74}$$

After some math, it can be shown that

$$F = F_1 + iF_2 = (\gamma_{1,1} + \gamma_{2,2}) + i(\gamma_{2,1} - \gamma_{1,2}) \tag{2.75}$$

and

$$G = G_1 + iG_2 = (\gamma_{1,1} - \gamma_{2,2}) + i(\gamma_{2,1} + \gamma_{1,2}) \ . \tag{2.76}$$

The quantities F and G are called *first and second flexion*, respectively. It is easy to show that D_{ijk} can be written in terms of F and G. Thus, they describe second order distortions of the images of lensed sources. Note that F is a spin-1 vector field. Indeed, it is

$$\vec{F} = \vec{\nabla}\kappa \ . \tag{2.77}$$

Thus, it describes transformations that are invariant under rotations by 2π. For this reason, F stretches the images along one particular direction, introducing asymmetries in their shape. On the contrary, G is a spin-3 tensor field. The transformations described by G are invariant under rotations by $2\pi/3$. This is manifested in the "triangular" pattern in the image shapes, as shown in Fig. 2.3.

2.6 Occurrence of images

The deflection of light rays causes a delay in the travel-time of light between the source and the observer. This time delay has two components:

$$t = t_{\rm geom} + t_{\rm grav} \tag{2.78}$$

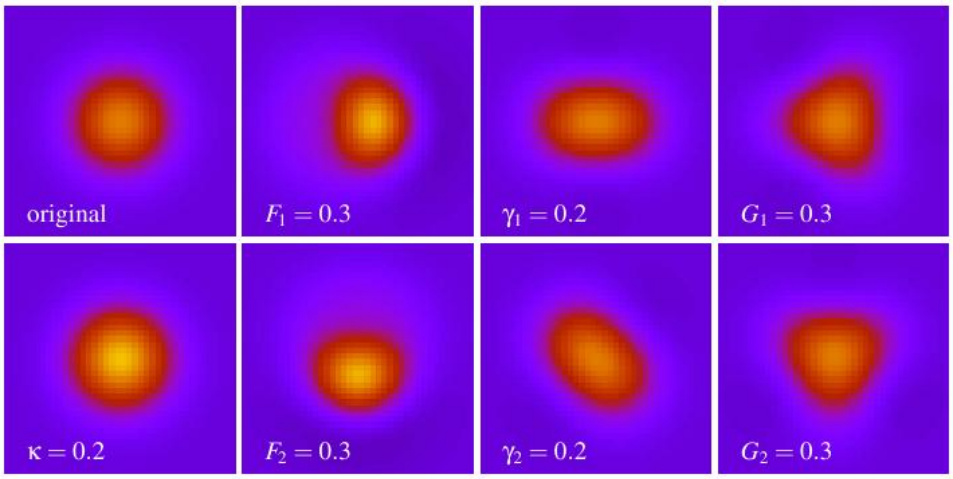

Figure 2.3: First and second order distortions on the image of a circular source. The unlensed source is shown in the top left panel. The convergence simply changes the size (bottom left panel). While the shear deforms the image such that it becomes elliptical (third column of panels from the left), the first and the second flexion introduce curvature and other distortions (second and fourth columns). Courtesy of Peter Melchior.

The first one has a geometrical reason and is due to the different path length of the deflected light rays compared to the unperturbed ones. This time delay is proportional to the squared angular separation between the intrinsic position of the source and the location of its image. The second one is the Shapiro delay encountered in Sect. 1.2. It was derived by comparing the time required to light to travel through a space-time with an effective refractive index and through empty space, by assuming *same trajectories*. it was found to be:

$$t_{\rm grav} = -\frac{2}{c^3}\int \Phi {\rm d}z \tag{2.79}$$

Using the definition of the lensing potential, this can be written as

$$t_{\rm grav} = -\frac{D_{\rm L} D_{\rm LS}}{D_{\rm S}}\frac{1}{c}\hat{\Psi}\ . \tag{2.80}$$

The geometrical term can be derived from the metric, but it can be estimated also through a simple geometrical construction, shown in Fig. 2.4. The extra-path of the light in presence of the lens can be written as

$$\Delta l = \xi\frac{\hat{\vec{\alpha}}}{2} = (\vec{\theta}-\vec{\beta})\frac{D_{\rm L} D_{\rm LS}}{D_{\rm S}}\frac{\vec{\alpha}}{2} = (\vec{\theta}-\vec{\beta})^2\frac{D_{\rm L} D_{\rm LS}}{2D_{\rm S}}\ , \tag{2.81}$$

and the corresponding time-delay is

$$t_{\rm geom} = \frac{\Delta l}{c} \tag{2.82}$$

Both the time delays occur at the lens position, thus they need to be multiplied by a factor $(1+z_{\rm L})$ for accounting for the expansion of the universe. Then, the total time

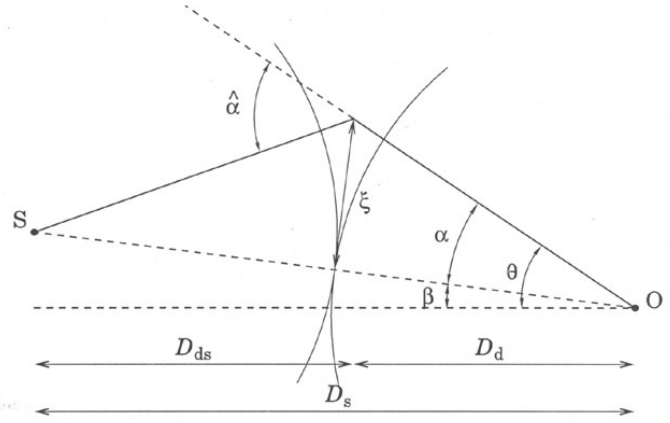

Figure 2.4: Illustration of the geometrical time delay.

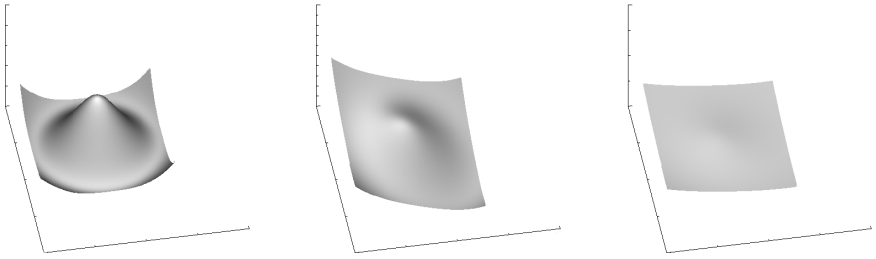

Figure 2.5: Time delay surfaces of an axially symmetric lens for three different source positions. Right panel: source and lens are perfectly aligned along the optical axis; middle panel: the source is no more aligned with the lens. Its projected position on the lens plane is moved along the line $x_1 = x_2$; right panel: the source is moved to an even larger angular distance from the optical axis.

delay introduced by gravitational lensing at the position $\vec{\theta}$ on the lens plane is[1]

$$t(\vec{\theta}) = \frac{(1+z_{\mathsf{L}})}{c}\frac{D_{\mathsf{S}}D_{\mathsf{L}}}{D_{\mathsf{LS}}}\left[\frac{1}{2}(\vec{\theta}-\vec{\beta})^2 - \Psi(\vec{\theta})\right] \ . \tag{2.83}$$

Through the effective lensing potential, the lens equation can be written as

$$(\vec{\theta}-\vec{\beta}) - \nabla\Psi(\vec{\theta}) = \nabla\left[\frac{1}{2}(\vec{\theta}-\vec{\beta})^2 - \Psi(\vec{\theta})\right] = 0 \ . \tag{2.84}$$

Eqs. (2.83) and (2.84) imply that images satisfy the Fermat Principle, $\nabla t(\vec{\theta}) = 0$. Images therefore are located at the stationary points of the time delay surface given by Eq. (2.83). The Hessian matrix of this surface is

$$T = \frac{\partial^2 t(\vec{\theta})}{\partial\theta_i\partial\theta_j} \propto (\delta_{ij} - \Psi_{ij}) = A \tag{2.85}$$

We can distinguish between three types of image:

[1] The adimensional form of the time delay can be obtained by multiplying and dividing by the factor $(\xi_0/D_{\mathsf{L}})^2$.

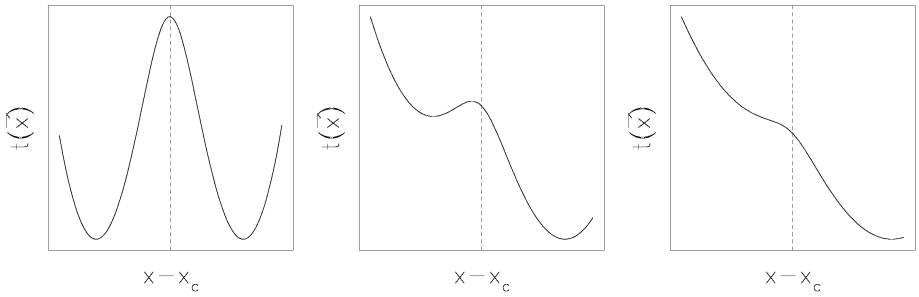

Figure 2.6: Profiles of the time delay surfaces displayed in Fig. (2.5) along the line $x_1 = x_2$.

(1) type I images arise at the minima of the time delay surface, where the eigenvalues of the Hessian matrix are both positive, hence $\det A > 0$ and tr$A > 0$. Therefore, they have positive magnification;

(2) type II images arise at the saddle points of the time delay surface, where eigenvalues have opposite signs. Since $\det A < 0$, they have negative magnification. The interpretation of a negative μ is that the parity of the image is flipped compared to the source;

(3) finally, type III images arise at the maxima of the time delay surface. Here, the eigenvalues are both negative, hence $\det A > 0$ and tr$A < 0$. These images therefore have positive magnification.

Since the Hessian matrix describes the local curvature of the time delay surface, the smaller is the curvature along one direction at the position where the image forms, the larger is its magnification along the same direction. We display in Fig. (2.5) some examples of the time delay surface for a general axially symmetric lens with core. The density profile of this lens scales with radius as r^{-2} outside the core. The surfaces are plotted for three different source position $\vec{\beta}$: in the left panel the source and the lens are perfectly aligned along the optical axis passing through the lens center ($\vec{y} = 0$ and $\vec{\theta} = 0$); in the middle and right panel, the source is moved far away, increasing its angular distance from the optical axis. In order to better see where the minima and the maxima arise, we show in Fig. (2.6) the profile along the line $x_1 = x_2$ of the same surfaces. When the source and the lens are perfectly aligned, the minima of the time delay surface are located on a ring and the maximum is at the lens center. The source therefore is mapped to a ring image of type I (the so called *Einstein Ring*) and to a central type III image. This last one is generally demagnified, since the curvature of the time delay surface here is large for density profiles peaked at the lens center.

As the source is moved far away from the optical axis, the time delay surface deforms. In particular, the ring breaks, leading to the formation of a minimum and of a saddle point. Three images therefore arise. In the case displayed in the middle panel of Fig. (2.5), the type I image at the minimum and the type II image at the saddle point are stretched in the tangential direction, since the local curvature of the time delay surface is small in that direction. This explains the formation of tangential arcs in galaxy clusters. However, as the source is moved to even larger angular distances from the optical axis, the saddle point and the maximum move much closer to each other, while the minimum follows the source. The local curvature of the time delay surface in the radial direction becomes smaller between the saddle point and the maximum as they get closer. The images arising at this two points therefore are stretched towards each other. Then a

radial image forms. When the saddle point and the maximum point touch, two images disappear and only the image arising at the minimum of the time delay surface remains (see right panels of Fig. (2.5) and Fig. (2.6)).

Here follows a number of other important properties of the time-delay surface:

- the height difference at different images of the surface $t(\vec{\theta})$ gives the difference in arrival time between these images. This time delay can be measured if the source is variable, and provides one way of potentially measuring the Hubble constant;
- in absence of the lens, the time-delay surface is a parabola which has a single extremum (a minimum); additional extrema have to come in pairs, thus the total number of images must be odd (as we showed earlier by continously deforming the time-delay surface);
- when two additional images are formed, they must be a maximum and a saddle point; in between them, the curvature changes from negative to positive, thus it is zero between them; remember that $\det A = 0$ is the condition for having a critical point, where the magnification is (formally) infinite. The critical lines thus separate multiple-image pairs; these pairs merge and desappear (as discussed above) at the critical lines. In other words, the critical lines separate regions of different image multiplicities.